Colloids and Surfaces A: Physicochemical and Engineering Aspects 680 (2024) 132629

Contents lists available at ScienceDirect

Colloids and Surfaces A: Physicochemical and Engineering Aspects

journal homepage: www.elsevier.com/locate/colsurfa

Modifying pickering polymerized high internal phase emulsion morphology by adjusting particle hydrophilicity

Enes Durgut [a,b], Muchu Zhou [c], Betül Aldemir Dikici [d], Reza Foudazi [c], Frederik Claeyssens [a,b,*]

[a] Kroto Research Institute, Department of Materials Science and Engineering, University of Sheffield, Sheffield, United Kingdom
[b] Department of Materials Science and Engineering, INSIGNEO Institute for in Silico Medicine, The University of Sheffield, Sheffield, United Kingdom
[c] School of Sustainable Chemical, Biological and Materials Engineering, The University of Oklahoma, Norman, OK, 73019, USA
[d] Department of Bioengineering, Izmir Institute of Technology, Urla, Izmir 35433, Turkey

HIGHLIGHTS

- Particle hydrophilicity affects HIPE morphology, viscosity, and the resulting PolyHIPE morphology.
- PolyHIPEs with either a closed or open cellular morphology can be obtained by adjusting the hydrophilicity of the particles.
- Dissolved particles act as macromolecular surfactants, resulting in PolyHIPEs with small but semi-open pores.
- HIPE viscosity can serve as an indicator of the openness of PolyHIPEs.
- The openness of PolyHIPEs decreases when dilatational interfacial elasticity decreases due to a reduction in hydrophilicity.

GRAPHICAL ABSTRACT

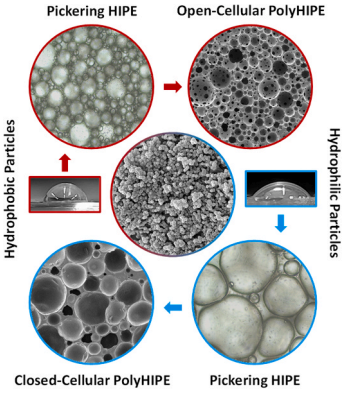

ARTICLE INFO

Keywords:
Pickering emulsions
Rheology
Arrested coalescence
Particles
HIPE
PolyHIPE

ABSTRACT

This study investigates the use of submicron polymeric particles with varying crosslinking densities as the sole stabilizer for producing Polymerized High Internal Phase Emulsions (PolyHIPE). We establish a direct correlation between the crosslinking density and the hydrophilicity of the polymer particles. The hydrophilicity of these particles significantly influences the morphology and rheology of HIPEs. These differences manifest as various morphological variations in the resulting PolyHIPE templates. It was discovered that by increasing the crosslinker weight percentage in the particles from 0 % to 100 %, PolyHIPEs with semi-open, open, and closed porous structures can be obtained. Furthermore, non-crosslinked particles were observed to dissolve in the continuous phase, acting as macromolecular surfactants that generate small pores akin to surfactant-stabilized structures in PolyHIPE. These findings offer fresh insights into the relationship between particle localization at the interface, HIPE rheology, and the formation of pore throats in Pickering PolyHIPEs, leading to the creation of either closed or open porous networks. Additionally, interfacial rheological results demonstrate that particles synthesized with varying monomer-to-crosslinker ratios exhibit different interfacial elasticities, which are linked to PolyHIPE morphology.

* Corresponding author at: Kroto Research Institute, Department of Materials Science and Engineering, University of Sheffield, Sheffield, United Kingdom.
E-mail address: f.claeyssens@sheffield.ac.uk (F. Claeyssens).

https://doi.org/10.1016/j.colsurfa.2023.132629
Received 28 August 2023; Received in revised form 14 October 2023; Accepted 19 October 2023
Available online 21 October 2023

1. Introduction

Polymerized High Internal Phase Emulsions (PolyHIPEs) are highly porous polymeric materials created using the emulsion templating method. This method relies on the production of a stable emulsion and its subsequent polymerization, which requires the use of emulsion stabilizers. Traditionally, surfactants serve as the stabilizers for the emulsion, resulting in templates with small pores (1–50 μm) and interconnected pore throats that connect adjacent pores. [1,2]. Alternatively, colloidal particles can be employed to stabilize emulsions, known as Pickering emulsions. Since the successful production of Pickering PolyHIPEs in 2007 by Menner et al. [3], there has been a growing interest in replacing surfactants with colloidal particles due to their efficiency in emulsion stabilization [4,5] and their functional properties [6,7]. Pickering PolyHIPEs are recognized for their larger pore sizes compared to conventional PolyHIPEs but lack pore throats [8–10]. Although the formation of pore throats in PolyHIPEs has not been fully elucidated, the closed porous structure of Pickering PolyHIPEs is attributed to a thick interfacial polymer film that separates neighboring pores, unlike conventional PolyHIPEs, which resist rupturing during or after polymerization [11,12]. While a closed cellular morphology is advantageous in applications requiring encapsulation, it limits their use in applications where an interconnected porous structure is necessary. For instance, applications involving diffusion, mass transfer, or cell ingrowth require such interconnected porous structures [13–15].

While Pickering PolyHIPEs are often associated with their closed cellular morphology, there have been a few reports demonstrating an interconnected pore structure. For instance, to achieve a stable Pickering HIPE, colloidal particles are typically subjected to surface modifications to adjust their hydrophilicity. This enables the particles to be situated at the oil/water interface and serve as emulsion stabilizers. Several reports have shown that the degree of surface modification influences the openness of the resulting templates, ranging from closed to interconnected porous structures [16–18]. Additionally, Zhang et al. reported that the use of sulfonated styrene particles as a HIPE stabilizer results in open and closed cellular morphologies when the continuous phase consists of butyl acrylate and styrene, respectively [19]. Assuming that particle-monomer interactions are minimal in the mentioned studies, both the degree of surface modification of particles and changes in the hydrophilicity of the continuous phase are factors influencing particle localization at the oil/water interface. Therefore, we hypothesize that the localization of particles at the oil/water interface can be a determining factor in the openness of Pickering PolyHIPEs.

The 2-ethylhexyl acrylate/isobornyl acrylate/trimethylolpropane triacrylate (EHA/IBOA/TMPTA) blend is a commonly used monomer blend for PolyHIPE production due to its tunable mechanical properties and ease of manufacture. EHA/IBOA/TMPTA PolyHIPEs have found applications in various fields, such as protein immobilization [20], serving as scaffolds for bone tissue engineering [21] and in the development of microfluidic devices for osteogenesis-on-a-chip [22]. Recently, two noteworthy developments have further enhanced the utility of EHA/IBOA/TMPTA PolyHIPEs as model porous materials. First, a straightforward method for surface functionalization via orthogonal photo click chemistry has been established [23]. Second, the successful formulation of HIPE-based resin for vat polymerization with commercial 3D printers has been achieved [24] which was further coated with nickel to obtain highly porous metal-based lattice structures [25]. Given the simplicity of manufacturing these PolyHIPEs, they can also serve as model systems for advancing our understanding and testing new hypotheses in emulsion templating.

Recently, we explored the use of IBOA/TMPTA microparticles as the sole HIPE stabilizer to produce an open cellular morphology in EHA/IBOA/TMPTA Pickering PolyHIPEs. This observation led us to propose a new mechanism for pore throat formation in Pickering PolyHIPEs: the partial but arrested coalescence of emulsion droplets. Additionally, we investigated the impact of the internal phase ratio, particle size, and particle concentration on PolyHIPE morphology and openness [26]. However, we did not evaluate the effect of particle hydrophilicity on this proposed mechanism. In this study, we aim to investigate the influence of particle hydrophilicity on HIPE morphology, rheology, interfacial viscoelasticity of the emulsions, and Pickering PolyHIPE morphology. We achieved this by using particles with varying compositions of TMPTA, ranging from 100 % IBOA to 100 % TMPTA. Tuning the TMPTA concentration in the particles allows us to modulate their hydrophilicity, as TMPTA is inherently hydrophilic. This approach enables us to examine the impact of particle hydrophilicity on the aforementioned parameters without requiring additional surface modifications.

2. Experimental

2.1. Materials

EHA, IBOA, TMPTA, Tween 20, potassium persulfate (KPS), and 2-hydroxy-2-methylpropiophenone (photoinitiator, PI) were purchased from Sigma-Aldrich (Poole, UK).

2.2. Nomenclature of Samples

The particles are designated with codes like IBxTMy, where x and y represent the weight percentages of IBOA and TMPTA used in particle synthesis, respectively. The prefix before the particle code, either (h) or (p), indicates whether it's associated with HIPE or PolyHIPE, respectively. For instance, (p)$IB_{75}TM_{25}$ signifies a PolyHIPE templated from an emulsion stabilized by particles containing 75 % wt IBOA and 25 % wt TMPTA.

2.3. IBOA microparticle synthesis

The particles were prepared through ultrasound-assisted emulsion polymerization. The continuous phase was created by dissolving 0.5 % wt of Tween 20 % and 0.2 % wt of KPS in water, using magnetic stirring at 500 RPM for 5 min. Subsequently, 2 g of the internal phase, consisting of an IBOA/TMPTA blend, and 18 g of the continuous phase were combined in a 40 mL plastic tube. The emulsion was formed by subjecting this mixture to ultrasonication at 100 Watts and 30 kHz using a Hielscher UP100H ultrasonicator for 2 min. The resulting emulsion droplets were thermally polymerized in a convection oven at 65 °C for 16 h. The polymer particles obtained were washed with 30 mL of methanol and then centrifuged at 14,000 RPM for 15 min. This washing process was repeated twice. After removing the methanol, the particles were suspended in 40 mL of water and dried in a convection oven at 65 °C for 24 h.

2.4. The preparation of PolyHIPE

The continuous phase was prepared by mixing 4 g of EHA/IBOA/TMPTA (63/21/16 % wt) and 0.2 g of IBOA/TMPTA particles through ultrasonication at 100 Watts and 30 kHz for one minute. Subsequently, 0.1 g of photoinitiator were added to the monomer/particle mixture. The internal phase, consisting of 16 g of deionized water, was added to the continuous phase using a syringe pump operating at a rate of 0.8 mL/min, while the system was mixed at 500 RPM (Pro40, SciQuip). During the emulsification process, the rotor blade was continuously adjusted to the top position as the emulsion volume increased. All the HIPEs were prepared within a span of 24 min. The resulting HIPEs were transferred to a glass petri dish and polymerized using a belt conveyor UV curing system (GEW Mini Laboratory, GEW Engineering UV) within one minute.

2.5. Preparation of thin films

Thin films were prepared with the same composition of particles for conducting water contact angle measurements. One gram of monomer blends was mixed with 0.025 g of PI. The monomer blend was squeezed between two glass slides and photopolymerized using the UV curing system.

2.6. Characterization

The IBOA/TMPTA particles were mounted onto double-sided carbon tape and coated with an 8 nm thick layer of gold. Subsequently, the particles were imaged using a scanning electron microscope (Inspect F, FEI) with a 5 kV accelerating voltage and a 3 μm spot size. The sizes of 200 particles were manually measured from the SEM images using ImageJ software. The polydispersity index of the particles was calculated using the following formula:

$$PDI = \left(\frac{\sigma}{D_p}\right)^2 \quad (1)$$

Where σ is the standard deviation of droplet size and $D_p$is the average droplet size.

A sessile drop test was performed to measure the water contact angle on polymer films with the same particle composition cast onto a glass slide. Glass slides were positioned on a flat surface, and images were captured using a smartphone (RedMI 10, Xiaomi) mounted on a tripod from a distance of approximately 2 cm from the samples. The images were subsequently analyzed using ImageJ software, with the assistance of the LB-ADSA plugin [27]. The average emulsion droplet size was determined by measuring the diameter of 100 droplets using ImageJ software. These measurements were taken from optical micrographs (CX43, Olympus) of freshly prepared HIPEs.

To deduce the molecular weight of the dissolved IBOA, we employed gel permeation chromatography (GPC) (Viscotek GPCmax VE 2001, Malvern Panalytical). The $IB_{100}TM_0$ particles were first dissolved in the continuous phase, and the mixture was then centrifuged at 14,000 RPM for 5 min to collect a gel-like IBOA. This collected gel-like IBOA was subsequently mixed with tetrahydrofuran (THF) before conducting the GPC measurement. For the dissolved $IB_{100}TM_0$ particles, 1 H nuclear magnetic resonance (NMR) spectra were recorded using an NMR spectrometer (Avance AVIII 400 MHz NMR, Bruker) operating at 400.13 MHz. A 30° pulse for excitation was used, with 64 k acquisition points over a spectral width of 20 ppm, 16 transients, and a relaxation delay of 1 s

The rheological tests included step flow and frequency sweep tests, which were conducted using a rheometer (AR2000, TA Instruments) with a cross-hatched steel plate (60 mm, 2°) at 25 °C. The applied shear rate ranged from 10 to 0.1 s^{-1} during the step flow test, and the frequency ranged from 10 to 0.1 Hz during the frequency sweep test. The skeletal density of PolyHIPEs was characterized using a pycnometer (AccuPyc 1340, Micromeritics). The porosity ($P_\varnothing$) of the samples was determined by subtracting the skeletal density (ρ_{sd}) from the calculated bulk density (ρ_c) using the following formula [28]:

$$P_\varnothing = \left(1 - \frac{\rho_{sd}}{\rho_c}\right)100 \quad (2)$$

The bulk density (ρ_c) was calculated based on a cylindrically molded EHA/IBOA/TMPTA monolith, which had a composition similar to the continuous phase of the HIPEs. This value was then used to determine the porosity according to Eq. (2).

To characterize the pore size of the PolyHIPEs, the diameter of 200 pores was measured from SEM images obtained using the same procedure as for the SEM imaging of particles. Since the PolyHIPE samples contain micron-sized pores, they were excluded from the measurement by acquiring images at lower magnifications (500x for (p)$IB_{100}TM_0$ and 100x for the remaining samples). This was achieved by laser cutting the samples, which caused the polymer to melt and eliminated the smaller features. Additionally, a statistical correction factor was applied to reduce errors introduced during uneven sectioning of pores [29,30]. The median pore diameter, obtained from the mercury intrusion porosimeter (AutoPore V, Micrometrics), was used as the average pore throat size of the samples. This is because the pore size provided by the mercury intrusion porosimeter corresponds to the pore throat size in PolyHIPEs [2].

The dilatational rheology of the particle-adsorbed oil-water interface was characterized using an optical tensiometer (Attension KSV Instruments, Biolin Scientific) at room temperature. The pendant drop of the aqueous phase was oscillated in the continuous phase containing IBOA/TMPTA particles at various frequencies (0.05–0.5 Hz) to obtain measurements of interfacial tension variation. Since 0.2 g of IBOA/TMPTA particles, as used in the emulsion formulation, resulted in the continuous phase turning white and limited the observation of the pendant drop, a reduced quantity of 0.001 g of IBOA/TMPTA particles was used for all cases. Fig. S1 shows the transparent oil phase both without and with 0.0005 g and 0.001 g of IB_0TM_{100} particles. The amplitude was kept constant for all measurements.

3. Results

3.1. IBOA microparticles

SEM images of IBOA microparticles prepared through ultrasound-assisted emulsion polymerization are presented in Fig. 1. The particle size gradually increased from 199 to 211 nm as the TMPTA content in the particles increased from 0 % to 50 %. A further increase in TMPTA content resulted in a reduction in the average particle size, reaching 145 nm for $IB_{25}TM_{75}$ and 60 nm for IB_0TM_{100} (Fig. 2A). In contrast, the PDI of the particles gradually increased as the TMPTA content increased, peaking at $IB_{25}TM_{75}$ and then reducing to 0.12 in IB_0TM_{100}. Additionally, although the particles were predominantly spherical, complex nonspherical particles were occasionally observed, especially in $IB_{50}TM_{50}$ and $IB_{25}TM_{75}$. Similar amorphous-shaped particles were previously observed in a blend of styrene, methyl methacrylate, and acrylic acid and were attributed to the incompatibility between constituents and subsequent phase separation [31]. Given that TMPTA is a water-miscible and relatively hydrophilic component of the organic mixture, a similar mechanism might have contributed to increased PDI, particularly in $IB_{25}TM_{75}$, and the formation of nonspherical shapes.

Contact angle measurements on a thin polymer film, which shares the same composition as the particles, were conducted and are presented in Fig. 2B. These water contact angle measurements were performed on a polymer film instead of on the particles themselves to eliminate the influence of surface roughness on the water contact angle. The increase in TMPTA content in the polymer composition led to a reduction in the contact angle, decreasing from 93.5° ($IB_{100}TM_0$) to 54.0° (IB_0TM_{100}). The ability to adjust the water contact angle of the particles by varying the IBOA/TMPTA content allows for the investigation of particle hydrophilicity's impact on HIPE/PolyHIPE morphology without the need for surface modifications.

3.2. HIPE

3.2.1. The continuous phase

After the particles were dispersed in the continuous organic phase through sonication, the continuous phase transformed into an opaque whitish liquid, indicating the formation of a suspension. However, the dispersion of $IB_{100}TM_0$ resulted in a transparent liquid with an observed increase in the viscosity of the continuous phase compared to other particle-dispersed continuous phases (Fig. S2 A). It is known that the viscosity of particle dispersions increases with particle concentration due to heightened interparticle interactions [32,33] However, in this

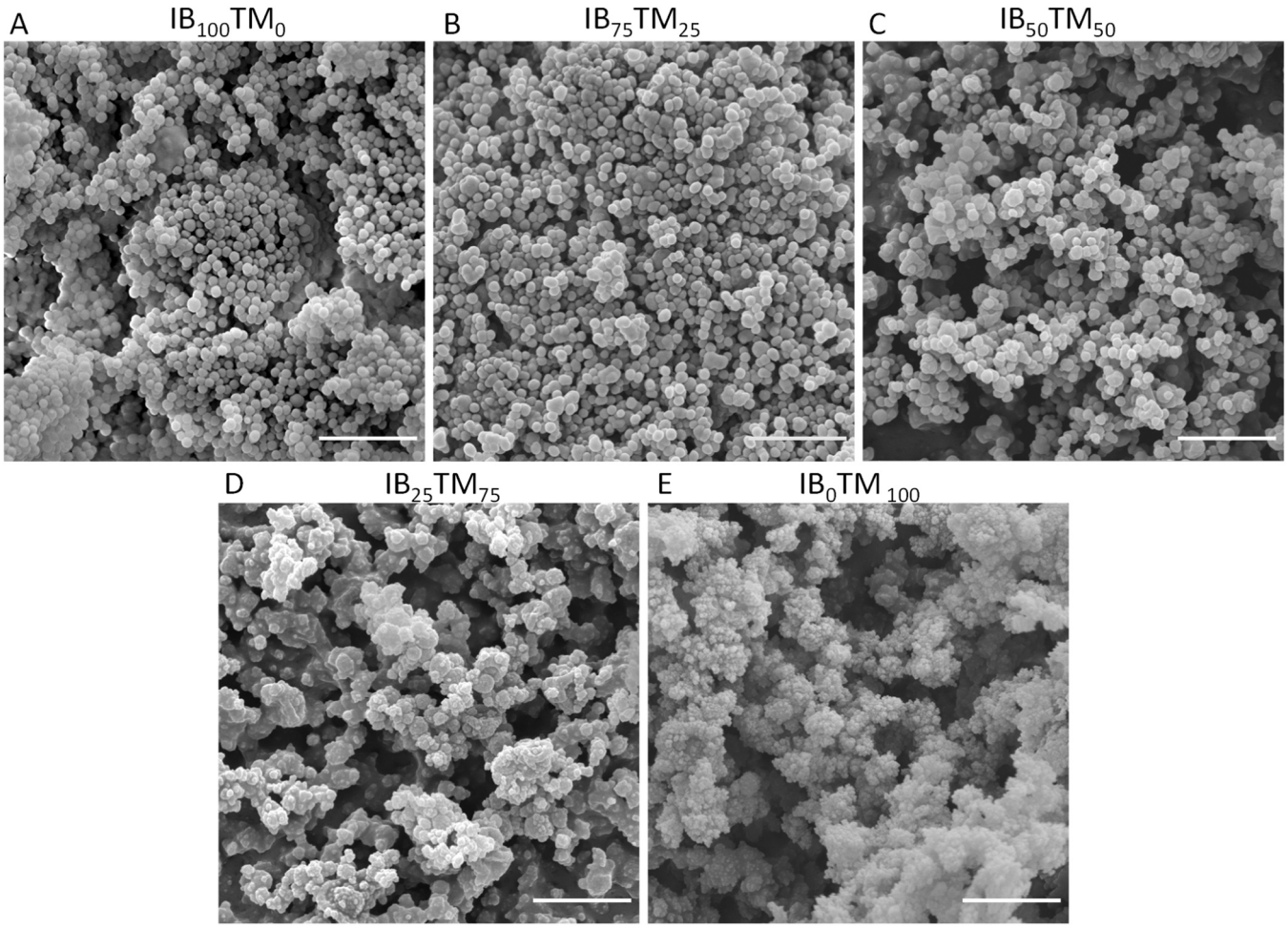

Fig. 1. SEM images of particles with various IBOA and TMPTA content: $IB_{100}TM_0$ (A), $IB_{75}TM_{25}$ (B), $IB_{50}TM_{50}$ (C), $IB_{25}TM_{75}$ (D) and IB_0TM_{100} (E). Scale bars are 2 μm.

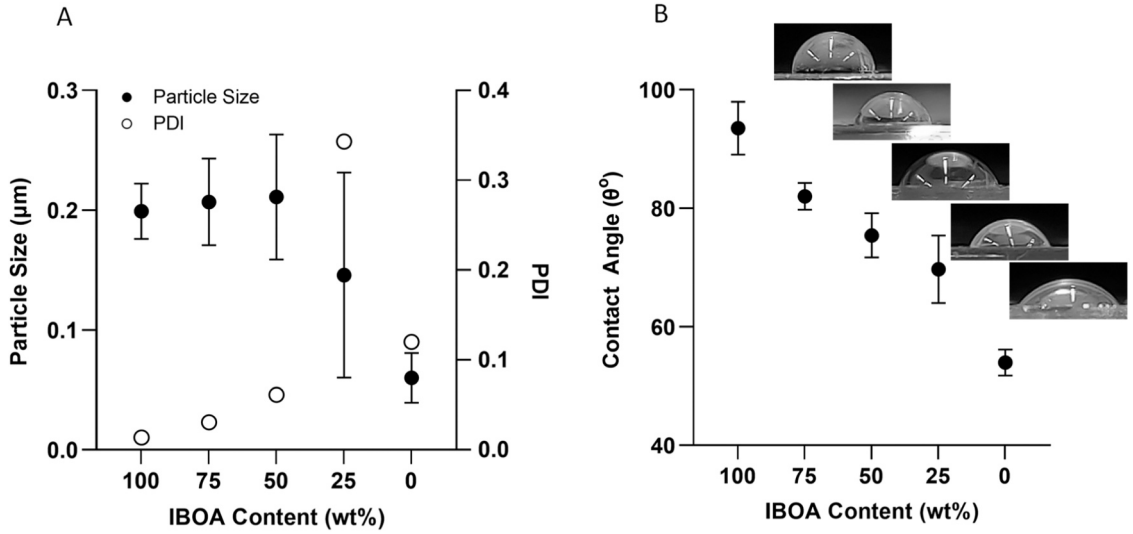

Fig. 2. The size and polydispersity index of IB-TM particles (A). The contact angle measurement of the thin polymeric film shares a similar composition with the IB-TM particles (B).

case, only the $IB_{100}TM_0$ dispersion exhibited a noticeable increase in viscosity, even though the particle concentration and average particle size were similar to $IB_{75}TM_{25}$ and $IB_{50}TM_{50}$. This phenomenon aligns with the observations made by *Tu et al.*, where a transparent-colored continuous phase with increased viscosity was previously noted when non-crosslinked styrene particles were dispersed in a styrene solution.

This effect was attributed to the swelling of particles within the continuous phase [34]. However, since $IB_{100}TM_0$ is not crosslinked, there is also the possibility that it might dissolve in the organic phase. To assess the dissolution of non-crosslinked IBOA, two cylindrical polymer monoliths were synthesized through free-radical polymerization (similar to PolyHIPE synthesis) with a composition similar to that of $IB_{100}TM_0$ and $IB_{75}TM_{25}$. These monoliths were kept in the EHA/I-BOA/TMPTA mixture. The $IB_{100}TM_0$ polymer cylinder completely dissolved within the organic mixture within 2 days (Fig. S2 B).

3.2.2. HIPE stability and droplets

The HIPEs were successfully prepared, and digital micrographs are presented in Fig. S3. A portion of the HIPEs was photopolymerized, while the remainder was kept at room temperature to observe emulsion stability. Within 15 min after preparation, visible large emulsion droplets were observed in (h)$IB_{25}TM_{75}$. Furthermore, (h)$IB_{25}TM_{75}$ experienced sedimentation and emulsion droplet coalescence within a week. This was an intriguing observation, as emulsions stabilized by particles with lower TMPTA content ($IB_{50}TM_{50}$) and higher TMPTA content (IB_0TM_{100}) did not exhibit observable emulsion instability for a week. Additionally, (h)$IB_{100}TM_0$ and (h)$IB_{50}TM_{50}$ only began to show sedimentation after 5 weeks.

HIPEs were imaged under a light microscope, and the optical micrographs are presented in Fig. 3. The average emulsion droplet sizes are provided in Table 1. It has been previously reported that emulsion droplet size correlates with particle size [35]. However, the emulsions in this experimental setup do not conform to this rule. (h)$IB_{100}TM_0$ exhibited significantly smaller emulsion droplets with an average size of ~14 μm, despite the particle size of $IB_{100}TM_0$ being similar to $IB_{75}TM_{25}$ and $IB_{50}TM_{50}$. Such small emulsion droplets are typically observed in surfactant-stabilized HIPE emulsions. This discrepancy may be attributed to the dissolution of $IB_{100}TM_0$ particles within the continuous phase, where they function as a macro-molecular surfactant rather than a typical Pickering stabilizer. Consequently, (h)$IB_{100}TM_0$ should be evaluated separately from the rest of the samples. Additionally, the smallest particle, IB_0TM_{100}, produced emulsions with the largest average droplet size of 146 μm. This is intriguing since previous reports have shown that emulsion droplet size correlates well with various sizes of $IB_{75}TM_{25}$ particles (ranging from 100 to 700 μm) [26]. The highest PDI of emulsion droplets was observed in (h)$IB_{25}TM_{75}$, approximately equal to 1. The reduced uniformity of emulsion droplets in (h)$IB_{25}TM_{75}$ might be due to a combination of the high PDI of $IB_{25}TM_{75}$ particles and the reduced stability of the HIPE. Furthermore, emulsion droplets in all samples appear spherical, except for (h)IB_0TM_{100}, which exhibits deformed spherical emulsion droplets, typically observed in Pickering HIPEs (Fig. 3E).

3.2.3. Rheology of HIPE

The rheological properties of the samples were measured, and the analyzed results are presented in Fig. 4. The frequency sweep results (Fig. S4) clearly indicate that all samples exhibit $G' > G''$ at all frequencies, confirming solid-like behavior, as expected for HIPEs with a unimodal droplet size distribution [36]. The viscosity of HIPE samples as a function of shear rate is provided in Fig. 4A. An increase in TMPTA content from 25 % to 75 % in the particles results in a reduction in viscosity. This trend is expected since the increase in emulsion droplet

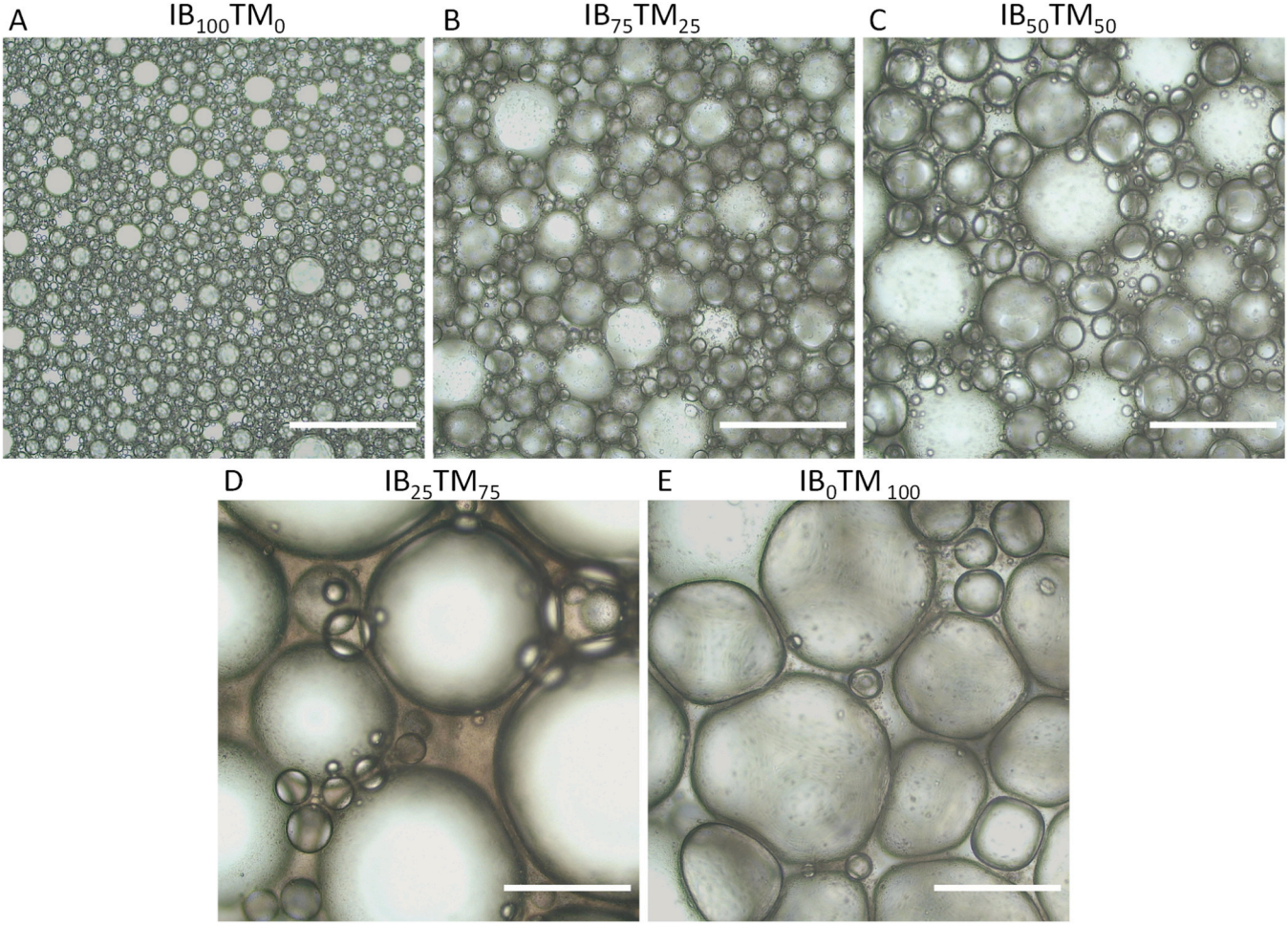

Fig. 3. Optical micrographs of HIPEs stabilized by IB-TM particles demonstrating the emulsion droplet size and the droplet shape. Scale bars are 200 μm.

Table 1
Skeletal density (ρ_{sd}), porosity ($P_{\varnothing}$), emulsion droplet size (d), polydispersity index of emulsion droplet size (*PDI d*), pore size (P_p), polydispersity index of pore size (*PDI* P_p), pore throat size (P_t), and relative pore throat size (P_t/P_p) of PolyHIPEs.

Sample	ρ_{sd} (g/cm3)	$P_{\varnothing}$	d (μm)	*PDI d*	P_p (μm)	*PDI* P_p	P_t (μm)	P_t / P_p
(p)$IB_{100}TM_0$	0.94	75.04	14.32	0.40	23.68	0.34	3.31	0.14
(p)$IB_{75}TM_{25}$	1.03	77.49	44.82	0.39	72.12	0.40	17.37	0.24
(p)$IB_{50}TM_{50}$	1.03	77.72	58.12	0.58	79.21	0.44	23.29	0.29
(p)$IB_{25}TM_{75}$	1.02	78.58	114.09	1.02	148.36	1.22	58.27	0.39
(p)IB_0TM_{100}	0.33	28.64	146.57	0.40	205.46	0.42	N/A	N/A

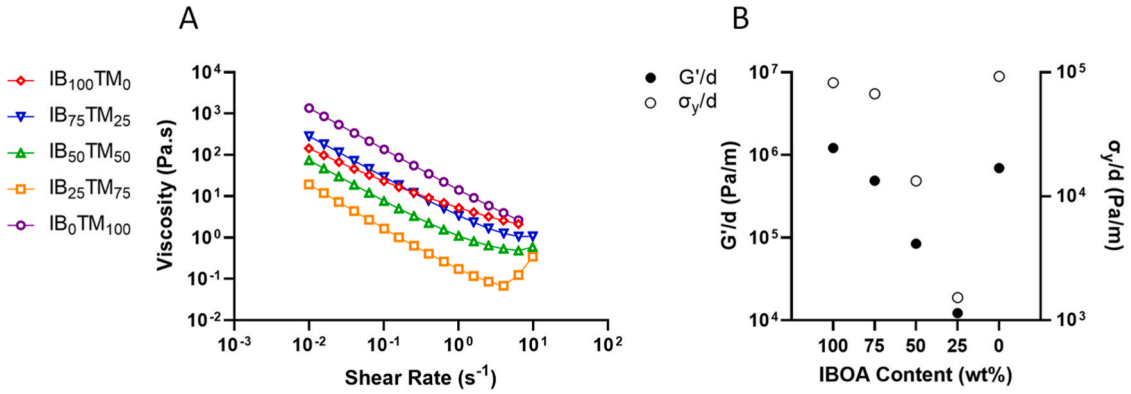

Fig. 4. The viscosity of HIPE samples as a function of shear rate obtained from step flow test (A) and, scaled elastic modulus (G′) and yield stress (σ) of HIPE samples obtained from frequency sweep test (B).

size leads to a decrease in viscosity when the internal phase volume of the HIPEs remains the same [29,32]. However, IB_0TM_{100} exhibits the highest viscosity despite having the largest emulsion droplets (Fig. 4). The observed increase in viscosity for (h)$IB_{25}IB_{75}$ between 1 and 10 s^{-1} is attributed to phase separation of the sample during the measurement. This is because this particular sample is less stable compared to the other HIPE samples.

The elastic properties of HIPEs scale with Laplace pressure, which is calculated as the interfacial tension divided by the droplet size. This holds true when the contribution of interdroplet interaction and interfacial rheology to bulk elasticity is negligible [37]. The prepared HIPEs have relatively large droplet sizes, on the order of tens of micrometers, where the effect of interdroplet interaction is very negligible. Determining the effective interfacial tension when particles are at the interface is not straightforward. Therefore, we compare the elastic properties by scaling them with droplet size, as shown in Fig. 4B. In other words, we divide the shear modulus (obtained from the G′ plateau in frequency sweep data) and yield stress (obtained by fitting the Herschel-Bulkley model) by droplet size to better illustrate the effect of interfacial phenomena. To draw a meaningful conclusion, (h)$IB_{100}TM_0$ should be excluded from the comparison due to the dissolution of particles in the continuous phase. For samples with stable particles, the trend is not monotonic. (h)IB_0TM_{100} exhibits the highest scaled shear modulus and yield stress among the Pickering HIPE samples, indicating that the effective interfacial tension in this sample is the highest and/or the interfacial rheology is responsible for the observed trend. This observation is further discussed in Section 3.4 and attributed to the effective interfacial tension.

It is well-established that under similar experimental conditions, Pickering HIPEs exhibit higher viscosity compared to surfactant-stabilized HIPEs due to attractive interparticle interactions, excluded volume effects, and attractive lateral capillary interactions [38]. Additionally, previous reports have shown that Pickering HIPEs have elastic moduli that are several orders of magnitude higher than surfactant-stabilized HIPEs [38,39]. In our previous work, we examined the rheological behavior of HIPEs stabilized by Hypermer B246 (a surfactant), $IB_{75}TM_{25}$, and silica (a commonly used colloidal stabilizer). We found that Hypermer B246 and $IB_{75}TM_{25}$ stabilized HIPEs exhibited comparable viscosity, while silica-stabilized HIPEs had higher viscosity despite having significantly larger droplet sizes than both Hypermer B246 and $IB_{75}TM_{25}$-stabilized HIPEs. The distinctive properties of (h)$IB_{75}TM_{25}$ and its atypical morphology (interconnected porous) were attributed to the localization of particles at the interface. $IB_{75}TM_{25}$ particles were predominantly observed around the pore throats in the PolyHIPE, rather than being distributed on the pore surface. Therefore, we concluded that the prevention of coalescence of emulsion droplets was not due to the typical particle shielding of droplets but rather the jamming of particles at the necking region of initially coalesced emulsion droplets. This phenomenon provided intermediate viscosity and droplet size compared to Hypermer B246 and silica-stabilized HIPEs [26].

In the case of (h)$IB_{75}TM_{25}$, (h)$IB_{50}TM_{50}$, and (h)$IB_{25}TM_{75}$ samples, their behavior aligns with our previous report. Within these three samples, as the TMPTA content in the particles increases, the droplet size also increases, leading to a decrease in viscosity and emulsion stability. However, this observed trend is not followed in the case of (h)IB_0TM_{100}. In (h)IB_0TM_{100}, we observe typical Pickering HIPE properties, including large and deformed-spherical emulsion droplets. Despite being stabilized by smaller particles, this sample exhibits increased viscosity as well as improved emulsion stability. The transition from atypical properties ((h)$IB_{75}TM_{25}$, (h)$IB_{50}TM_{50}$, and (h)$IB_{25}TM_{75}$) to typical properties ((h) IB0TM100) can be attributed to the particle hydrophilicity in the given experimental setup.

3.3. PolyHIPE

3.3.1. The porous structure

PolyHIPEs from IB/TM particle-stabilized HIPEs were successfully prepared, and the properties of PolyHIPEs are listed in Table 1. Both the skeletal density and the porosity of the samples are nearly the same, with no significant differences, except for (p)IB_0TM_{100}. Since the skeletal density is the density of the material composing the PolyHIPE skeleton, it should be the same within all the samples. Additionally, since the internal phase volume was equal in all the HIPE samples, the porosity of

the samples should also be the same. Therefore, the reduced skeletal density obtained by the pycnometer and the accordingly calculated reduced porosity of (p)IB_0TM_{100} indicate a closed porous structure. This suggests that gas could not penetrate into the closed porous structure of (p)IB_0TM_{100}, thus, the skeletal density was underestimated. Additionally, the bulk densities of all the samples were measured as approximately 0.22 g/cm^3.

Particle hydrophilicity had a major impact on the porous structure as well as on the number-averaged pore size distribution of the Pickering PolyHIPEs, as shown in Fig. 5. The pore sizes and their uniformity in the PolyHIPEs correlate with the emulsion droplets observed in optical micrographs. (p)$IB_{100}TM_0$ has the smallest average pore size at 23.7 μm. As discussed in the previous section, the stabilization of the HIPE is likely due to dissolved IBOA particles functioning as a macromolecular surfactant. The dissolution of non-crosslinked particles in the continuous phase and its effect on maximum internal phase uptake have been previously observed [40]. This was confirmed by Hua et al., who reported that yet-to-be-dissolved particles were functioning as a stabilizer, while the dissolved particles were forming the skeleton of the porous material [41]. However, to our knowledge, this is the first time that surfactant-stabilized-grade small pore sizes in Pickering PolyHIPEs have been obtained by utilizing the dissolution of colloidal particles as an emulsion stabilizer. While (p)$IB_{100}TM_0$ exhibits pores with a few pore throats (Fig. 5A), there are occasionally observed but extremely large and interconnected pores as well (Fig. S5). These atypical pores might be due to being stabilized by yet-to-be-dissolved $IB_{100}TM_0$ particles, and their existence might depend on both the standing time of the HIPE or the sonication duration during the particle dispersion within the continuous phase. (p)IB_0TM_{100} is the only Pickering PolyHIPE exhibiting conventional Pickering PolyHIPE morphology: closed and large pores compared to conventional surfactant-stabilized PolyHIPEs. The pores in (p)IB_0TM_{100} samples exhibit a deformed spherical morphology, which correlates well with the corresponding HIPE optical micrographs (Fig. 5E).

3.3.2. The Microstructure

All the IBOA-TMPTA blend particle-stabilized HIPE templates exhibit an interconnected porous structure (Fig. 5B–D). In our previous study [26], we attributed pore throat formation under the current experimental conditions to arrested coalescence. Similarly, both pore throats and pore-pore junctions were densely covered with particles, providing evidence of pore throat formation due to the partial coalescence of emulsion droplets that were subsequently arrested by particle jamming. The interconnected porous structure of Pickering PolyHIPEs, except for (p)IB_0TM_{100}, has been confirmed, and the average pore throat size and distribution have been obtained through mercury intrusion porosimetry (Fig. 6). The pore throat size of the samples correlates with the pore size. (p)$IB_{100}TM_0$ exhibits a bimodal pore throat size distribution with peaks at approximately 1 and 6 μm. The second peak at around 6 μm might be attributed to the occasionally observed extremely large and interconnected pores of (p)$IB_{100}TM_0$. (p)$IB_{25}TM_{75}$ is another sample exhibiting a bimodal pore throat size distribution, which is expected since (p)$IB_{25}TM_{75}$ also exhibits a bimodal pore size distribution.

SEM images of PolyHIPEs focusing on the pore surface and interface are presented in Fig. 7. In (p)$IB_{100}TM_0$, a smooth pore surface is observed, with particles sporadically observed on the polymer wall but

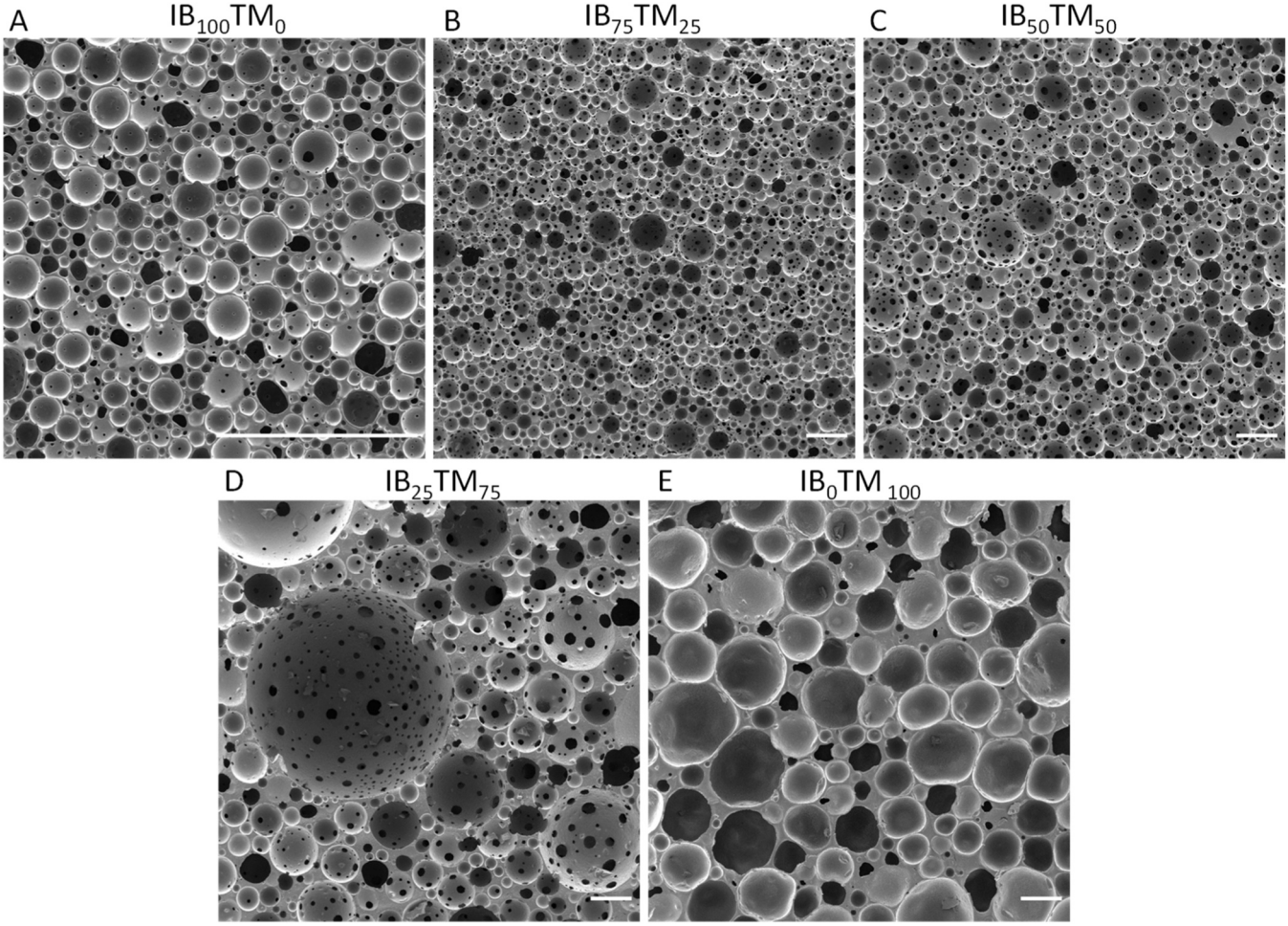

Fig. 5. SEM images of laser-cut PolyHIPEs, templated from IB-TM-stabilized HIPEs demonstrating the overall porous structure (A–E). Scale bars are 250 μm.

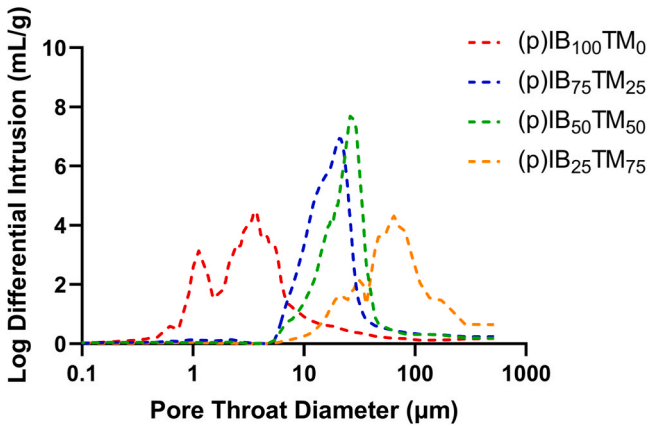

Fig. 6. The obtained pore throat diameter (μm) from mercury intrusion porosimeter as a function of log differential intrusion (mL/g).

not on the pore surface itself (Fig. 7A). Both (p)$IB_{75}TM_{25}$ and (p)$IB_{50}TM_{50}$ exhibit similar micromorphology, with submicron pore throats especially noticeable on the relatively smaller pores. These submicron pore throats are hypothesized to result from the arrested coalescence of nearby micron-sized pores (Fig. 7B-C). The micron-sized pores are also found at the pore-pore interface. Pores in these samples have both smooth and rough patches on their surfaces due to embedded particles. Pore throats and pore-pore junctions exhibit a similar morphology, densely covered with particles. In contrast, (p)$IB_{25}TM_{75}$ shares the micromorphology seen in other IBOA/TMPTA blends, except for the pore surface. In (p)$IB_{25}TM_{75}$, relatively large interconnected pores exhibit roughness, while relatively smaller pores have smooth surfaces (Fig. 7D). Finally, (p)IB_0TM_{100} exhibits a solid polymer film that separates neighboring pores (Fig. 7E). In this case, regardless of pore size, the pores have rough surfaces similar to the large pore surfaces of (p)$IB_{25}TM_{75}$.

Considering that IB_0TM_{100} particles are the most hydrophilic among the particles, making them expected to be wetted more by the internal water phase, it's not surprising to observe these particles located towards the void (pore surface). However, the similar localization of $IB_{25}TM_{75}$ particles on the large, interconnected pores of (p)$IB_{25}TM_{75}$ remains unexplained.

Additionally, the effect of leftover Tween 20 on particles is also considered. IB100TM0 particles were dissolved in deprotonated chloroform, and NMR analysis was conducted to evaluate whether Tween 20 was adsorbed onto the particles. The NMR results showed Tween 20 remnants on the IB100TM0 particles, with a molar ratio of 1–0.15. However, the impact of Tween 20 remnants should be minimal for several reasons. First, Tween 20 is a hydrophilic surfactant that preferentially stabilizes oil-in-water emulsions. Second, even if all Tween 20 were absorbed onto the particle surface during particle synthesis, the overall weight percentage of Tween 20 in the continuous phase would be 0.25 %. Experiments showed that neither 0.25 % nor 5 % wt of Tween 20

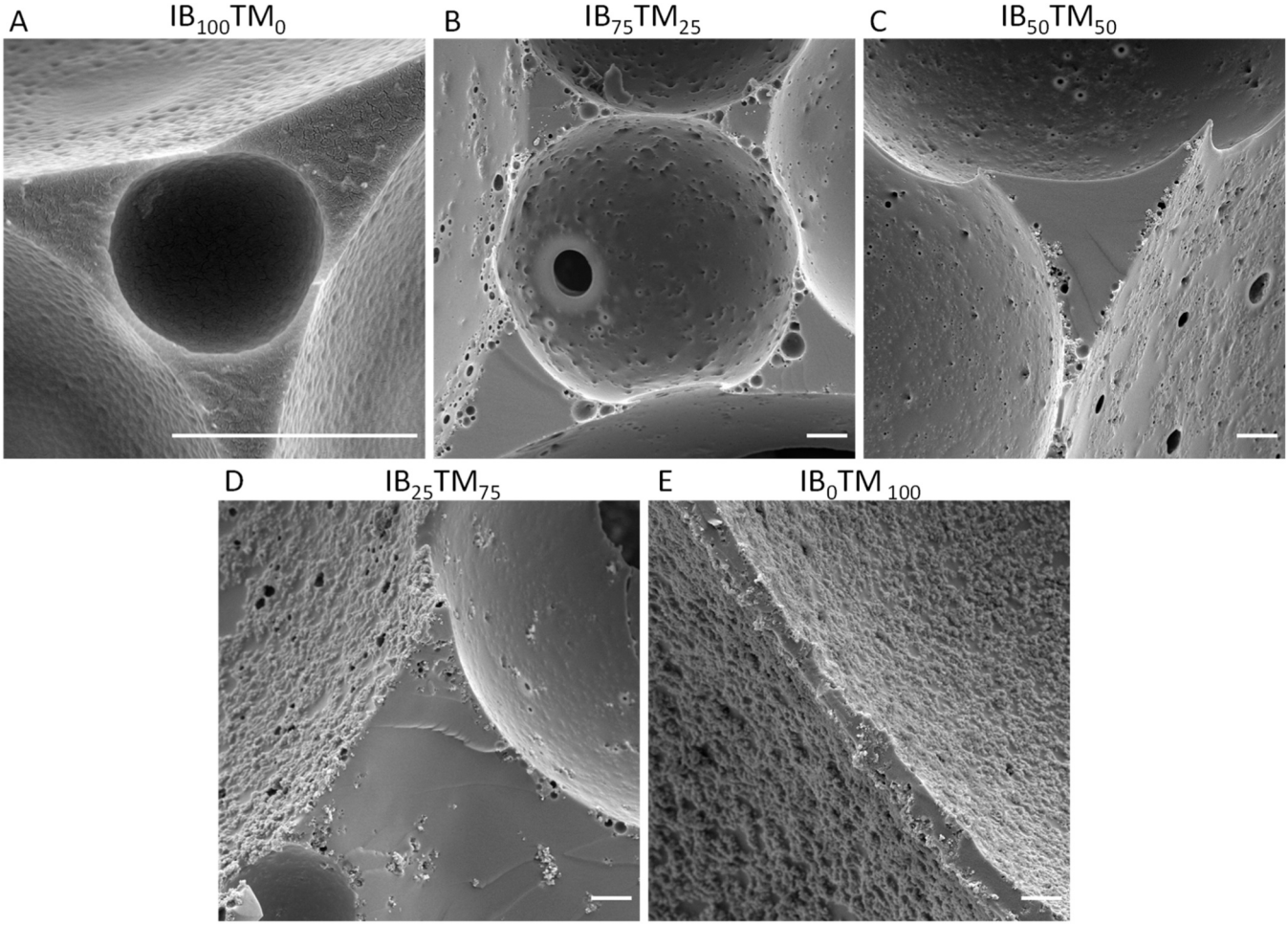

Fig. 7. The microstructure of PolyHIPE samples. The smooth pore surface and the polymer interface separate pores from each other (A). Pore surface with smooth and rough regions, submicron pore throats, and micron-sized pores at the close vicinity of larger pores (B and C). The rough and the smooth pore surface of large and small pores, respectively (D). Polymeric film separates two pores and the rough surface of pores (E). Scale bars are 2.5 μm.

in the continuous phase is able to stabilize the given HIPE. Finally, all the particles were prepared with the same amount of Tween 20; however, both HIPE and PolyHIPE samples exhibit significant rheological and morphological differences.

3.4. Interfacial rheology

The dilatational interfacial rheology was performed to investigate the effect of interfacial rheology in the presence of different particles on the morphology of PolyHIPEs. The dilatational modulus (E) is defined as follows [42,43]:

$$E = A_0 \frac{\Delta\gamma}{\Delta A} \tag{3}$$

where A_0 is the pendant drop interface area, ΔA is the interface area difference, and $\Delta\gamma$ is the interfacial tension difference because of the volume oscillation. The dilatational elastic modulus (E′) and viscous modulus (E″) are defined as follows [43]:

$$E = |E|\cos(\phi) + i|E|\sin(\phi) = E' + iE'' \tag{4}$$

where ϕ is the phase angle, $E' = |E|\cos(\phi)$, and $E'' = |E|\sin(\phi)$. The interfacial tension and interface area oscillation are fitted with a sinusoidal function to obtain the interfacial moduli. Fig. S6 shows the typical normalized pendant drop interface area and interfacial tension oscillation curves at 0.5 Hz and 0.1 Hz for the blank interface (i.e., in the absence of particles), respectively. As seen, the blank interface also shows dilatational rheological properties, which can be attributed to the surface activity of monomers and crosslinkers. Fig. S6A shows the aqueous phase drop immersed in the clear continuous phase containing 0.001 g of $IB_{100}TM_0$, whereas Fig. S7B is the aqueous phase drop immersed in the translucent continuous phase containing 0.001 g of IB_0TM_{100}. The typical normalized oscillation curves for 0.001 g $IB_{100}TM_0$-adsorbed interface, to which different waiting times were applied, are provided in Fig. S8. Fig. S9 shows the typical normalized oscillation curves for the 0.001 g IB_0TM_{100}-adsorbed interface. Without applying the waiting time, the $IB_{100}TM_0$-stabilized interface is already viscoelastic (Fig. S8A), indicating quick adsorption of $IB_{100}TM_0$ at the interface. Nevertheless, for IB_0TM_{100} particle with 0 h waiting time, the shape of the pendant drop almost remains the same during oscillation, and the interfacial tension does not show any oscillation (Fig. S9A), demonstrating the adsorption of particles at the interface in Pickering HIPEs has a slower kinetics compared to soluble polymers.

The measurements were performed after different waiting times, as

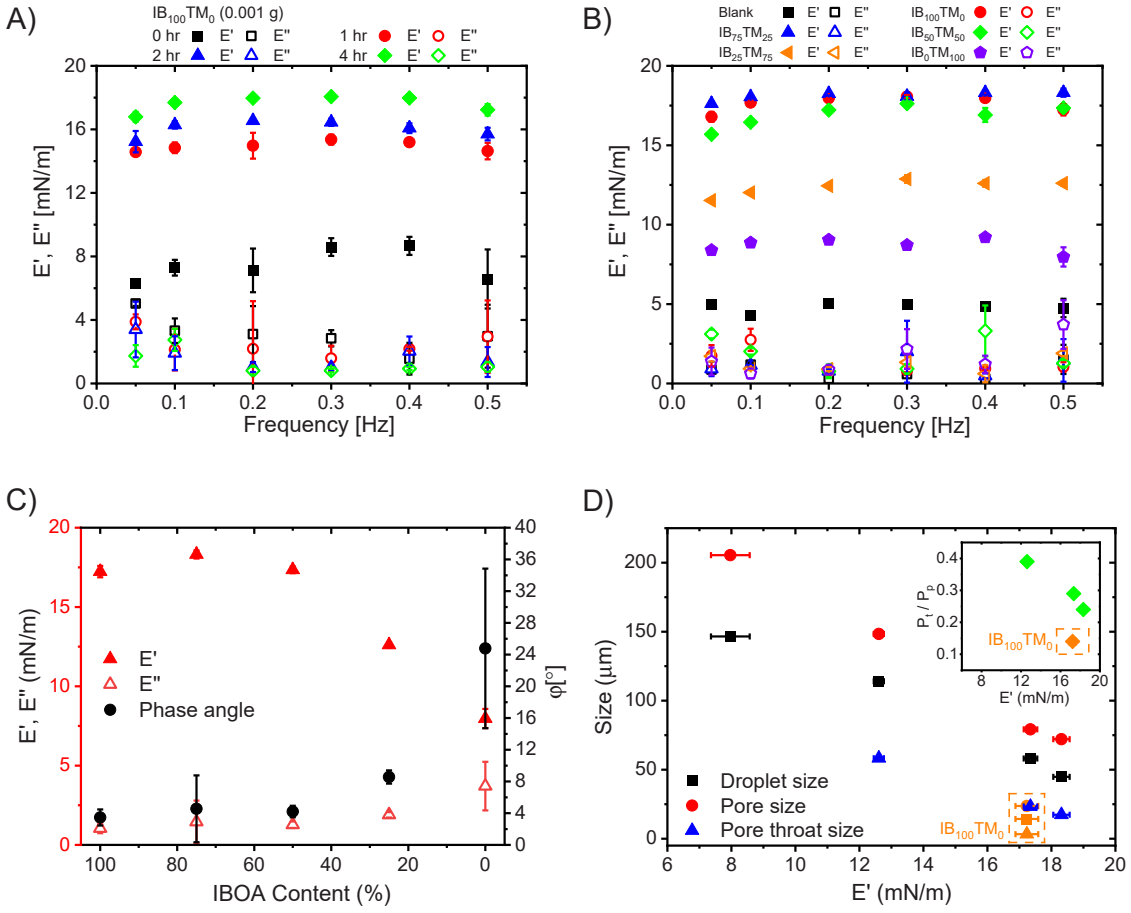

Fig. 8. (A) E′ and E″ of 0.001 g $IB_{100}TM_0$ particle-adsorbed oil-water interface when applying different waiting times of 0, 1, 2, and 4 h. (B) Dilatational elastic and viscous moduli of 0.001 g IBOA/TMPTA particles-adsorbed oil-water interface after 4 h waiting. The black points are the moduli of the blank interface. The interfacial elastic modulus decreases as decreasing the amount of monomer IBOA in particle synthesis, whereas the interfacial viscous modulus remains unchanged as varying the ratio of IBOA and TEMPTA. Additionally, both interfacial elastic and viscous moduli of IBOA/TMPTA particles-adsorbed oil-water interface are independent of frequency. (C) Dilatational rheological properties of 0.001 g IBOA/TMPTA particles-adsorbed oil-water interface at 0.5 Hz frequency after 4 h waiting. The black solid points show the phase angle, which is dependent on IBOA content. The red solid points are the elastic modulus, which decreases with lowering IBOA except for the case of 100 % of IBOA (soluble polymer). The red hollow points are the viscous modulus, which is independent of the IBOA content. (D) HIPE droplet size, PolyHIPE pore size, and PolyHIPE pore throat size as a function of dilatational elasticity. The inset shows the P_t / P_p versus interfacial elasticity. The orange points are for $IB_{100}TM_0$ particles, which do not follow the trend due to their solubility in the continuous phase.

mentioned earlier, from the drop formation moment to evaluate the interfacial rheological properties in the equilibrium state (i.e., minimizing transient effects). Fig. S7A typically shows the E′ and E″ of $IB_{100}TM_0$-stabilized interface with different waiting times of 0, 1, 2, and 4 h at varied frequencies, indicating that the E′ increases as the age of the interface increases. However, the E″ remains almost the same regardless of the waiting time. As mentioned earlier, different waiting times, including 0, 1, 2, 4, and over 12 h are applied before oscillation for particle IB_0TM_{100}, as seen in Fig. S10. The E' increases over time also for the IB_0TM_{100} interface (see Fig. S10 inset), although the increase is smaller compared to that of the $IB_{100}TM_0$ interface. The results suggest that a 4 h waiting time is a good approximation of equilibrium interfacial rheology.

Fig. 8B shows the E′ and E″ of the oil-water interface in the presence of 0.001 g IBOA/TMPTA particles after applying 4 h of waiting at varied frequencies. The interfacial moduli of all samples are independent of the frequency. For blank interface, E′ is higher than E″, and the introduction of IBOA/TMPTA particles further increases the elasticity of the interface while the viscous contribution remains unchanged. For particles synthesized with less amount of IBOA, the interfacial elastic modulus of the oil-water interface is lower, while no change in the viscous contribution is observed. The interfacial rheological properties are a function of the particle's hydrophilicity, shape, size, and aggregates [44–48]. Since all of these characteristics change among $IB_{75}TM_{25}$, $IB_{50}TM_{50}$, $IB_{25}TM_{75}$, and IB_0TM_{100} particles ($IB_{100}TM_0$ was excluded as it dissolves in the continuous phase), it is impossible to attribute the observed changes in interfacial rheology to the characteristics of the particles.

Fig. 8C shows the E′ and E″ of the interface with 0.001 g of different IBOA/TMPTA particles at 0.5 Hz after waiting for 4 h. As supporting information, the interfacial moduli at 0.05 Hz are provided in Fig. S11. The IBOA/TMPTA particles-adsorbed interface is an elastic-dominated interface with E′ higher than E″ at both 0.5 Hz and 0.05 Hz, and the E″ is almost independent of the IBOA content. It should be mentioned that E′ is lower for particles synthesized with less amount of IBOA. However, $IB_{100}TM_0$ is an exception because these particles are dissolved in the continuous phase and act similarly to macromolecular emulsifiers rather than Pickering stabilizers. Additionally, the phase angle increases with a decrease in IBOA content, as seen in Fig. 8B, indicating that the interface becomes more viscous for particles synthesized with less IBOA concentration [43]. According to Fig. 2B, lower IBOA content increases the hydrophilicity of IBOA/TMPTA particles. However, since the particle positioning at the interface depends on the surface properties of both aqueous and oil phases, it is unclear how this phenomenon increases interfacial viscoelasticity shown in Fig. 8C. Nevertheless, the formation of closed-cell structure, as seen in Fig. 5E, may be attributed to the increase of interfacial viscoelasticity [49]. We hypothesized that the non-monotonic trend observed in Fig. 4 for Pickering HIPEs is due to the changes in interfacial tension and/or interfacial rheology. However, Fig. 8C shows that the interfacial rheology data has a monotonic trend when the IBOA content of particle decreases from 75 % to 0 % (Pickering HIPEs). Therefore, the highest scaled modulus and yield stress for IB_0TM_{100} sample in Fig. 4 can be attributed to changes in effective interfacial tension rather than interfacial rheology.

Fig. 8D shows the HIPE droplet size, PolyHIPE pore size, and PolyHIPE pore throat size against interfacial elasticity. As seen, droplet, pore, and pore throat sizes decrease for higher interfacial elasticity. To cancel out the effect of pore size on the pore throat size, as discussed in the work of Zhou *et al.* [49], the P_t / P_p versus interfacial elasticity should be studied, as shown in the inset of Fig. 8D. Similar to surfactant stabilized HIPEs studied by Zhou et al. [49], the P_t / P_p ratio decreases when the interface elasticity decreases. It should be noted that the particle $IB_{100}TM_0$ is highlighted as the orange data points in Fig. 8D since they are dissolved in the continuous phase and are different from the rest of the IBOA/TMPTA particles.

4. Conclusion

We demonstrated the effect of particle hydrophilicity by tuning the crosslinker concentration in particles on Pickering PolyHIPE morphology. It was observed that particle hydrophilicity has a significant impact on emulsion stability, droplet size and shape, and rheology. HIPEs stabilized by particles with a water contact angle of 54° exhibit traditional Pickering HIPE behavior ((h)IB0TM100). On the other hand, HIPEs stabilized by particles with a water contact angle of 82–69° exhibit reduced droplet size, spherical droplets, and reduced viscosity, similar to traditional surfactant-stabilized HIPEs ((h)$IB_{75}TM_{25}$, (h)$IB_{50}TM_{50}$, and (h)$IB_{25}TM_{75}$). The difference in HIPE behavior is also reflected in the morphological differences in PolyHIPEs. It is concluded that it is possible to tune the openness of the PolyHIPE by adjusting the particle hydrophilicity from interconnected to closed porous structure. Additionally, IBOA/TMPTA particle-stabilized oil-water interfaces exhibit viscoelasticity, which is affected by the adsorption time, with the elastic modulus higher than the viscous modulus. Furthermore, lower IBOA content during particle synthesis results in a decrease in interfacial elasticity. Additionally, the dissolution of particles within the continuous phase, functioning as a macromolecular surfactant, is demonstrated, providing conventional PolyHIPE-grade small pores with a semi-open porous structure. These results support the previously proposed mechanism for pore throat formation in Pickering PolyHIPEs by arrested coalescence and provide new insights into the relationship between the mechanism and particle hydrophilicity. Since the rheology of the HIPEs is affected by particle hydrophilicity, and these changes are correlated with PolyHIPE openness, rheological measurements can be conducted to determine if the HIPE template would be interconnected or not.

The demonstrated surfactant-free Pickering PolyHIPEs can be used in applications such as tissue engineering and as catalyst supports due to their tunable pore and pore throat size. The research suggests an innovative approach that involves utilizing both hydrophilic and hydrophobic particles as emulsion stabilizers to achieve a tailored porous structure in PolyHIPE materials. When hydrophilic particles are employed, they tend to result in a closed porous structure while decorating the pore surfaces with particles. Conversely, the use of hydrophobic particles typically leads to an open-cellular morphology. By combining both types of particles as emulsion stabilizers, it becomes possible to potentially create a hybrid structure that features open-cellular pores while also being adorned with hydrophilic particles. This approach holds promise for offering unique advantages, especially in incorporating functional particles such as metal-organic frameworks. It enables a streamlined, one-pot synthesis method for crafting PolyHIPE materials with precisely engineered pore structures and surface decorations, opening up new possibilities for diverse applications.

CRediT authorship contribution statement

Enes Durgut: Conceptualization, Methodology, Validation, Investigation, Visualization, Writing – original draft. **Muchu Zhou:** Methodology, Validation, Visualization, Formal analysis, Writing – original draft. **Betul Aldemir Dikici:** Writing – review & editing. **Reza Foudazi:** Writing – review & editing, Supervision. **Frederik Claeyssens:** Writing – review & editing, Supervision.

Declaration of Competing Interest

The authors declare that they have no known competing financial interests or personal relationships that could have appeared to influence the work reported in this paper.

Data Availability

Data will be made available on request.

Acknowledgements

The authors gratefully acknowledge the Republic of Turkey-The Ministry of National Education for funding Enes Durgut. They also acknowledge the Engineering and Physical Sciences Research Council (Grant No. EP/I007695/1) and the Medical Research Council (Grant No. MR/L012669/1) for funding the equipment used in this study. Frederik Claeyssens also thanks the Royal Society for funding of a Royal Society Leverhulme Trust Senior Research Fellowship 2022 (SRF\R1\221053). We also acknowledge Dr. Christopher Holland for conducting bulk rheological measurements.

Supporting Information

Digital micrographs of particle dispersed continuous phases (Fig. S1-S2), dissolved $IB_{100}TM_0$ (Fig. S2), HIPE stability (Fig. S3); the frequency sweep graph (Fig. S4) and interconnected pore of (p)$IB_{100}TM_0$ (Fig. S5) and interfacial rheology-related figures mentioned in the text (Fig. S6-S11).

Appendix A. Supporting information

Supplementary data associated with this article can be found in the online version at doi:10.1016/j.colsurfa.2023.132629.

References

[1] H.H. Mert, PolyHIPE composite based-form stable phase change material for thermal energy storage, Int. J. Energy Res. 44 (2020) 6583–6594, https://doi.org/10.1002/er.5390.
[2] A. Barbetta, N.R. Cameron, Morphology and surface area of emulsion-derived (PolyHIPE) solid foams prepared with oil-phase soluble porogenic solvents: span 80 as surfactant, Macromolecules 37 (2004) 3188–3201, https://doi.org/10.1021/ma0359436.
[3] A. Menner, V. Ikem, M. Salgueiro, M.S.P. Shaffer, A. Bismarck, High internal phase emulsion templates solely stabilised by functionalised titania nanoparticles, Chem. Commun. (2007) 4274–4276, https://doi.org/10.1039/b708935j.
[4] B.R. Midmore, Colloids and a surfaces preparation of a novel silica-stabilized oil/water emulsion, Colloids Surf. A Physicochem. Eng. Asp. 132 (1998) 257–265.
[5] N. Bizmark, M.A. Ioannidis, Nanoparticle-stabilised emulsions: droplet armouring: Vs. droplet bridging, Soft Matter 14 (2018) 6404–6408, https://doi.org/10.1039/c8sm00938d.
[6] U. Azhar, C. Huyan, X. Wan, C. Zong, A. Xu, J. Liu, J. Ma, S. Zhang, B. Geng, Porous multifunctional fluoropolymer composite foams prepared via humic acid modified Fe3O4 nanoparticles stabilized Pickering high internal phase emulsion using cationic fluorosurfactant as co-stabilizer, Arab. J. Chem. 12 (2019) 559–572, https://doi.org/10.1016/j.arabjc.2018.04.003.
[7] Q. Wang, H. Ma, J. Chen, Z. Du, J. Mi, Interfacial control of polyHIPE with nano-TiO2 particles and polyethylenimine toward actual application in CO_2 capture, J. Environ. Chem. Eng. 5 (2017) 2807–2814, https://doi.org/10.1016/j.jece.2017.05.034.
[8] L.L.C. Wong, V.O. Ikem, A. Menner, A. Bismarck, Macroporous polymers with hierarchical pore structure from emulsion templates stabilised by both particles and surfactants, Macromol. Rapid Commun. 32 (2011) 1563–1568, https://doi.org/10.1002/marc.201100382.
[9] Y. Yang, Z. Wei, C. Wang, Z. Tonga, Lignin-based Pickering HIPEs for macroporous foams and their enhanced adsorption of copper(II) ions, Chem. Commun. 49 (2013) 7144–7146, https://doi.org/10.1039/c3cc42270d.
[10] I. Barbara, M. Dourges, Preparation of porous polyurethanes by emulsion-templated step growth polymerization, 132, 2017, pp. 243–251. https://doi.org/10.1016/j.polymer.2017.11.018.
[11] V.O. Ikem, A. Menner, T.S. Horozov, A. Bismarck, Highly permeable macroporous polymers synthesized from pickering medium and high internal phase emulsion templates, Adv. Mater. 22 (2010) 3588–3592, https://doi.org/10.1002/adma.201000729.
[12] W. Zhu, Y. Zhu, C. Zhou, S. Zhang, Pickering emulsion-templated polymers: Insights into the relationship between surfactant and interconnecting pores, RSC Adv. 9 (2019) 18909–18916, https://doi.org/10.1039/c9ra03186c.
[13] S. Dikici, B. Aldemir Dikici, S. Macneil, F. Claeyssens, Decellularised extracellular matrix decorated PCL PolyHIPE scaffolds for enhanced cellular activity, integration and angiogenesis, Biomater. Sci. 9 (2021) 7297–7310, https://doi.org/10.1039/d1bm01262b.
[14] B. Aldemir Dikici, M.C. Chen, S. Dikici, H.C. Chiu, F. Claeyssens, In vivo bone regeneration capacity of multiscale porous polycaprolactone-based high internal phase emulsion (PolyHIPE) scaffolds in a Rat Calvarial Defect Model, ACS Appl. Mater. Interfaces 15 (2023) 27696–27705, https://doi.org/10.1021/acsami.3c04362.
[15] S. Dikici, Ascorbic acid enhances the metabolic activity, growth and collagen production of human dermal fibroblasts growing in three-dimensional (3D) culture, Gazi Univ. J. Sci. 36 (2022) 1, https://doi.org/10.35378/gujs.1040277.
[16] W. Yi, H. Wu, H. Wang, Q. Du, Interconnectivity of macroporous hydrogels prepared via graphene oxide-stabilized pickering high internal phase emulsions, Langmuir 32 (2016) 982–990, https://doi.org/10.1021/acs.langmuir.5b04477.
[17] X. Zheng, Y. Zhang, H. Wang, Q. Du, Interconnected macroporous polymers synthesized from silica particle stabilized high internal phase emulsions, Macromolecules 47 (2014) 6847–6855, https://doi.org/10.1021/ma501253u.
[18] B. Pang, H. Zhang, M. Schilling, H. Liu, X. Wang, F. Rehfeldt, K. Zhang, High-internal-phase pickering emulsions stabilized by polymeric dialdehyde cellulose-based nanoparticles, 2020. https://doi.org/10.1021/acssuschemeng.0c01116.
[19] T. Zhang, Z. Xu, Q. Guo, Closed-cell and open-cell porous polymers from ionomer-stabilized high internal phase emulsions, Polym. Chem. 7 (2016) 7469–7476, https://doi.org/10.1039/c6py01725h.
[20] S.J. Pierre, J.C. Thies, A. Dureault, N.R. Cameron, J.C.M. Van Hest, N. Carette, T. Michon, R. Weberskirch, Covalent enzyme immobilization onto photopolymerized highly porous monoliths, Adv. Mater. 18 (2006) 1822–1826, https://doi.org/10.1002/adma.200600293.
[21] R. Owen, C. Sherborne, T. Paterson, N.H. Green, G.C. Reilly, F. Claeyssens, Emulsion templated scaffolds with tunable mechanical properties for bone tissue engineering, J. Mech. Behav. Biomed. Mater. 54 (2016) 159–172, https://doi.org/10.1016/j.jmbbm.2015.09.019.
[22] H. Bahmaee, R. Owen, L. Boyle, C.M. Perrault, A.A. Garcia-Granada, G.C. Reilly, F. Claeyssens, Design and evaluation of an osteogenesis-on-a-chip microfluidic device incorporating 3D cell culture, Front. Bioeng. Biotechnol. 8 (2020) 1–17, https://doi.org/10.3389/fbioe.2020.557111.
[23] J.P. Hooker, B. Parker, E. Wright, T. Junkers, N.R. Cameron, Photoresponsive emulsion-templated porous materials via orthogonal photoclick chemistry, ACS Appl. Mater. Interfaces 15 (2023) 11141–11149, https://doi.org/10.1021/acsami.2c22546.
[24] N. Sengokmen Ozsoz, S. Pashneh-Tala, F. Claeyssens, Optimization of a high internal phase emulsion-based resin for use in commercial vat photopolymerization additive manufacturing, 3D Print. Addit. Manuf. (2023), https://doi.org/10.1089/3dp.2022.0235.
[25] N. Sengokmen-Ozsoz, R. Boston, F. Claeyssens, Investigating the potential of electroless nickel plating for fabricating ultra-porous metal-based lattice structures using PolyHIPE templates, ACS Appl. Mater. Interfaces 15 (2023) 30769–30779, https://doi.org/10.1021/acsami.3c04637.
[26] E. Durgut, C. Sherborne, B. Aldemir Dikici, G.C. Reilly, F. Claeyssens, Preparation of interconnected pickering polymerized high internal phase emulsions by arrested coalescence, Langmuir (2022), https://doi.org/10.1021/acs.langmuir.2c01243.
[27] A.F. Stalder, T. Melchior, M. Müller, D. Sage, T. Blu, M. Unser, Low-bond axisymmetric drop shape analysis for surface tension and contact angle measurements of sessile drops, Colloids Surf. A Physicochem. Eng. Asp. 364 (2010) 72–81, https://doi.org/10.1016/j.colsurfa.2010.04.040.
[28] B. Aldemir Dikici, S. Dikici, F. Claeyssens, Synergistic effect of type and concentration of surfactant and diluting solvent on the morphology of highly porous emulsion templated tissue engineering scaffolds, Colloids Surf. B Biointerfaces (2022).
[29] B. Aldemir Dikici, F. Claeyssens, Basic principles of emulsion templating and its use as an emerging manufacturing method of tissue engineering scaffolds, Front. Bioeng. Biotechnol. 8 (2020), https://doi.org/10.3389/fbioe.2020.00875.
[30] B. Aldemir Dikici, A. Malayeri, C. Sherborne, S. Dikici, T. Paterson, L. Dew, P. Hatton, I. Ortega Asencio, S. MacNeil, C. Langford, N.R. Cameron, F. Claeyssens, Thiolene-and polycaprolactone methacrylate-based polymerized high internal phase emulsion (polyhipe) scaffolds for tissue engineering, Biomacromolecules 23 (2022) 720–730, https://doi.org/10.1021/acs.biomac.1c01129.
[31] Y. Zhu, S. Zhang, Y. Hua, H. Zhang, J. Chen, Synthesis of latex particles with a complex structure as an emulsifier of pickering high internal phase emulsions, Ind. Eng. Chem. Res. 53 (2014) 4642–4649, https://doi.org/10.1021/ie404009x.
[32] B.P. Binks, S.O. Lumsdon, Catastrophic phase inversion of water-in-oil emulsions stabilized by hydrophobie silica, Langmuir 16 (2000) 2539–2547, https://doi.org/10.1021/la991081j.
[33] V.O. Ikem, A. Menner, A. Bismarck, High internal phase emulsions stabilized solely by functionalized silica particles, ** Zuschriften (2008) 8401–8403, https://doi.org/10.1002/ange.200802244.
[34] S. Tu, C. Zhu, L. Zhang, H. Wang, Q. Du, Pore structure of macroporous polymers using polystyrene/silica composite particles as pickering stabilizers, Langmuir 32 (2016) 13159–13166, https://doi.org/10.1021/acs.langmuir.6b03285.
[35] B.P. Binks, S.O. Lumsdon, Pickering emulsions stabilized by monodisperse latex particles: effects of particle size, Langmuir 17 (2001) 4540–4547, https://doi.org/10.1021/la0103822.
[36] R. Foudazi, I. Masalova, A.Y. Malkin, The rheology of binary mixtures of highly concentrated emulsions: Effect of droplet size ratio, J. Rheol. (N. Y. N. Y) 56 (2012) 1299, https://doi.org/10.1122/1.4736556.
[37] R. Foudazi, S. Qavi, I. Masalova, A.Y. Malkin, Physical chemistry of highly concentrated emulsions, Adv. Colloid Interface Sci. 220 (2015) 78–91, https://doi.org/10.1016/j.cis.2015.03.002.
[38] M. Kaganyuk, A. Mohraz, Role of particles in the rheology of solid-stabilized high internal phase emulsions, J. Colloid Interface Sci. 540 (2019) 197–206, https://doi.org/10.1016/j.jcis.2018.12.098.
[39] E.S. Lee, D.G. Kim, K.H. Kim, Distinctive rheological properties of Pickering emulsions: from their origin to the applications, Korea Aust. Rheol. J. 34 (2022) 91–103, https://doi.org/10.1007/s13367-022-00018-x.

[40] S. Zhang, J. Chen, PMMA based foams made via surfactant-free high internal phase emulsion templates, Chem. Commun. (2009) 2217–2219, https://doi.org/10.1039/b819101h.
[41] Y. Hua, Y. Chu, S. Zhang, Y. Zhu, J. Chen, Macroporous materials from water-in-oil high internal phase emulsion stabilized solely by water-dispersible copolymer particles, Polym. (Guildf.) 54 (2013) 5852–5857, https://doi.org/10.1016/j.polymer.2013.08.055.
[42] V.N. Kazakov, E.L. Barkalova, L.A. Levchenko, T.M. Klimenko, V.B. Fainerman, R. Miller, Dilation rheology as medical diagnostics of human biological liquids, Colloids Surf. A Physicochem. Eng. Asp. 391 (2011), https://doi.org/10.1016/j.colsurfa.2011.03.028.
[43] H. Wang, X. Wei, Y. Du, D. Wang, Experimental investigation on the dilatational interfacial rheology of dust-suppressing foam and its effect on foam performance, Process Saf. Environ. Prot. 123 (2019), https://doi.org/10.1016/j.psep.2019.01.027.
[44] L. Yue, W. Pu, T. Zhao, J. Zhuang, S. Zhao, A high performance magnetically responsive Janus nano-emulsifier: preparation, emulsification characteristics, interfacial rheology, and application in emulsion flooding, J. Pet. Sci. Eng. 208 (2022), https://doi.org/10.1016/j.petrol.2021.109478.
[45] S. Reynaert, P. Moldenaers, J. Vermant, Interfacial rheology of stable and weakly aggregated two-dimensional suspensions, Phys. Chem. Chem. Phys. 9 (2007), https://doi.org/10.1039/b710825g.
[46] J. Wang, F. Yang, J. Tan, G. Liu, J. Xu, D. Sun, Pickering emulsions stabilized by a lipophilic surfactant and hydrophilic platelike particles, Langmuir 26 (2010), https://doi.org/10.1021/la903817b.
[47] R. Van Hooghten, V.E. Blair, A. Vananroye, A.B. Schofield, J. Vermant, J.H. J. Thijssen, Interfacial rheology of sterically stabilized colloids at liquid interfaces and its effect on the stability of pickering emulsions, Langmuir (2017), https://doi.org/10.1021/acs.langmuir.6b04365.
[48] E. Guzmán, L. Liggieri, E. Santini, M. Ferrari, F. Ravera, Effect of hydrophilic and hydrophobic nanoparticles on the surface pressure response of DPPC monolayers, J. Phys. Chem. C. 115 (2011), https://doi.org/10.1021/jp207713x.
[49] M. Zhou, R. Foudazi, Effect of cosurfactant on structure and properties of polymerized high internal phase emulsions (PolyHIPEs), Langmuir 37 (2021), https://doi.org/10.1021/acs.langmuir.1c00419.